Atmospheric Environment 125 (2016) 383–395

Contents lists available at ScienceDirect

Atmospheric Environment

journal homepage: www.elsevier.com/locate/atmosenv

Atmospheric SO_2 oxidation efficiency over a semi-arid region: Seasonal patterns from observations and GEOS-Chem model

Timmy Francis*, M.M. Sarin, R. Rengarajan

Physical Research Laboratory, Ahmedabad 380 009, India

HIGHLIGHTS

- Assess molar ratio of SO_4^{2-} to total SO_x ($SO_x = SO_2 + SO_4^{2-}$) at a high altitude site.
- Observed patterns are validated against GEOS-Chem model simulations.
- The ratios from field measurements as well as simulations exhibit a seasonality.
- Assess contributions from PBL, OH, RH, dust load, transport and dry deposition.

ARTICLE INFO

Article history:
Received 17 February 2015
Received in revised form 2 September 2015
Accepted 4 September 2015
Available online 10 September 2015

Keywords:
Sulphur dioxide
Sulphate
Atmospheric oxidation
GEOS-Chem
OH radical
Dry deposition

ABSTRACT

The oxidation efficiency of atmospheric SO_2, measured as a molar ratio of SO_4^{2-} to total SO_x ($SO_x = SO_2 + SO_4^{2-}$), referred as S-ratio, have been studied from a high altitude site (Gurushikhar, Mt. Abu: 24.6° N, 72.7° E, 1680 m ASL) in a semi-arid region of western India. A global 3-dimensional Chemical Transport Model (CTM), GEOS-Chem (v8-03-01), is employed to interpret the observed patterns. The S-ratios derived from time series SO_2 and SO_4^{2-} measurements exhibited a pronounced seasonality, with relatively low ratios in Feb–Mar 2010, high ratios in Nov–Dec 2009 and intermediate values in Sep–Oct 2009. The lower S-ratios for Feb ‘10 and Mar ‘10 (median values 0.10 and 0.08 respectively) have been attributed to the relatively high planetary boundary layer (PBL) heights – to reduce the SO_2 loss from the atmosphere via dry deposition – as well as the lower OH radical levels and low ‘aged air mass influx’ during these months. On the other hand, low PBL heights and significant long range transport contributions are projected to be the possible causes for the higher S-ratios during Nov ‘09 and Dec ‘09 (median values 0.30 and 0.28 respectively). The seasonal patterns for the S-ratios predicted by the CTM for the GEOS-Chem $4° \times 5°$ grid cell containing the sampling site showed highest ratios in Jul–Aug, and the lowest in Apr. The model has been employed further to study the contributions from various parameters to the S-ratios such as PBL, OH, RH, dust load, transport pattern and dry deposition. Sensitivity simulations showed the S-ratios enhancing with dust load with the peak in May (~4.7% (median)). Similarly, the ‘dry deposition’ is seen to boost the S-ratios with the peak in August (~66.3% (median)). Also, model simulations to assess the ‘altitudinal dependence of S-ratios’ have revealed a pronounced seasonal behaviour.

1. Introduction

The aerosol sulphate (SO_4^{2-}) formation in the atmosphere is predominantly via the oxidation of its precursor species sulphur dioxide (SO_2) (EPA I, 1996; EPA II, 1996), and proceeds through homogeneous as well as heterogeneous pathways. Studies by earlier workers (Hidy et al., 1978; Husar and Patterson, 1980) indicated that the molar ratio of SO_4^{2-} to total SO_x ($SO_x = SO_2 + SO_4^{2-}$), termed S-ratio, exhibit a seasonality. Further, Kaneyasu et al. (1995) showed that the S-ratio can be best used as a measure of the formation efficiency of SO_4^{2-} in the atmosphere. Miyakawa et al. (2007) suggested that the seasonal variation of S-ratio is linked to the seasonality in the boundary layer height and photochemical activity. They proposed that the higher planetary boundary layer for summer results in reduced loss rate of SO_2 via dry deposition which in turn causes an efficient oxidation of SO_2 to SO_4^{2-} before loss onto the surface, to enhance the S-ratio.

* Corresponding author. Geo-Sciences Division, Physical Research Laboratory, Ahmedabad 380 009, India.
E-mail address: dr.timmyfrancis@gmail.com (T. Francis).

http://dx.doi.org/10.1016/j.atmosenv.2015.09.021
1352-2310/

Similarly the production rate of OH radical – the major species responsible for the atmospheric oxidation process (Levy, 1971) – is influenced by the incoming solar radiation (insolation) intensity as well as the water vapour content. The seasonal changes in the transport pattern of polluted air and the resulting variability in the aged air mass input also could contribute to a seasonal variability in the S-ratio.

This paper presents a study assessing the seasonal patterns in S-ratios over a semi-arid region in western India. The analysis includes deriving monthly median S-ratios from field measurements of SO_2 and SO_4^{2-} and comparing with those from a global 3D chemical transport model (CTM), GEOS-Chem (v8-03-01).

A remote high altitude site (Gurushikhar, Mount Abu) was opted for the experimental study.

2. Materials and methods

2.1. Site description and meteorological parameters

The sampling site, Gurushikhar, Mt. Abu (24.6° N, 72.7° E, 1680 m ASL) is a remote high altitude mountain site in a semi-arid region of western India, with minimal local emissions. The region has an annual average rainfall of about 600–700 mm spread over Jul–Sep, during SW-monsoon. The site makes occasional entry into the free-tropospheric zone during post-monsoon (Oct–Nov) and winter (Dec–Feb) when the PBL is relatively low over the region (Francis, 2012). During the summer months (Mar–Jun) the site mostly gets accommodated within the PBL. The meteorological parameters during the sampling periods (wind speed, wind direction, relative humidity (RH), and air temperature) were recorded by an automatic weather station at the site (Fig. 1).

2.2. Experimental setup

The experimental set up for the SO_2 measurements are elaborated in Francis (2012) and is briefed here. A primary UV fluorescence SO_2 Monitor (Thermo – 43i TLE) was employed for the ambient SO_2 measurements. The performance evaluations of similar systems are reported elsewhere (Igarashi et al., 2004; Luke, 1997; Luria et al., 1992). The manufacturer claims that the Model 43i-TLE measures SO_2 at levels never before achieved, down to a 0.05 ppb level (300 s averaging time) (see http://www.thermoscientific.com/content/tfs/en/product/enhanced-trace-level-so-sub-2-sub-analyzer-model-43-i-i-i-tle.html). Calibrations were performed routinely with a standard SO_2 gas (2 ppmv with N_2 balance gas, Spectra, USA) and zero air, employing a dynamic gas calibrator (Thermo – 146i).

For the SO_4^{2-} measurements, fine mode aerosol samples were collected on Whatman cellulose filters (200 × 250 mm^2) employing a high volume air sampler (Thermo) with a flow rate of 1.12 m^3/min and a cut off diameter of 2.5 micron ($PM_{2.5}$) – in general three aerosol samples (sampling duration ~4 h) were collected during daytime and one sample (sampling duration ~12 h) during night time. Table 1 provides relevant details of the aerosol sampling, such as date of sample collection and the number of samples collected. In the analytical procedure for the measurement of sulphate (SO_4^{2-}) in the aerosol samples, one-fourth portion of the filter was soaked in 50 mL of Milli-Q water (18.2 MΩ resistivity) for 4 h during which ultrasonication was performed in steps of 5 min to a total of 20 min to extract water soluble ionic species (WSIS). In the water extracts, inorganic anions (Cl^-, NO_3^- and SO_4^{2-}) were measured on a Dionex ion chromatograph (Rastogi and Sarin, 2005; Rengarajan and Sarin, 2004). The anions were separated on Ionpac AS14A analytical column and AG14A guard column, in conjunction with an anion self-regenerating suppressor (ASRS), using 8.0 mM Na_2CO_3 – 1.0 mM $NaHCO_3$ as eluent. The measured Cl^-, NO_3^- and SO_4^{2-} concentrations were further corrected for procedural blanks (comprising of blank filters and analytical reagents).

2.3. Model description

The global 3-dimensional chemical transport model, GEOS-Chem (v8-03-01; http://acmg.seas.harvard.edu/geos/) with GEOS-5 assimilated meteorology was employed for this study. The GEOS-5 data have a temporal resolution of 6-h (3-h resolution for surface fields and mixing depths) and horizontal resolution of 0.5° latitude × 0.667° longitude, with 72 levels in vertical extending from surface to approximately 0.01 hPa. The model simulates HOx-NOx-VOC-ozone chemistry (Bey et al., 2001; Park et al., 2004) and elaborate simulation evaluations can be found elsewhere (Park et al., 2004; Wang et al., 2008; Fairlie et al., 2007; Chen et al., 2009).

The model was spun up for 12 months, from Jan 2008 to Jan 2009, starting from chemical climatology; this effectively removes the influence of initial conditions. The simulations were then conducted for Jan 2009–Apr 2010 at 4° × 5° resolutions. Unless mentioned otherwise, the standard input.geos file distributed with the GEOS-Chem codes (v8-03-01), specifying the various input parameters and emission inventories – EMEP (Vestreng and Klein, 2002), BRAVO (Kuhns et al., 2003), EDGAR (Olivier and Berdowski, 2001), Streets inventory (Streets et al., 2006), CAC (http://www.ec.gc.ca/pdb/cac/cac_home_e.cfm), and EPA/NEI05 – have been used, with only the simulation start/end dates and ND49 diagnostics – to generate the time series data – modified. Aerosol sources and processes used in the present simulation are as described by Park et al. (2006), with the addition of dust and sea salt as described by Fairlie et al. (2007) and Alexander et al. (2005). Wet deposition of soluble aerosols and gases follows the scheme of Liu et al. (2001) including contributions from scavenging in convective updrafts, rainout, and washout. Dry deposition follows a standard resistance-in-series model (Wesely, 1989). The model outputs were analysed using global atmospheric model analysis package (GAMAP) (Version 2.15; http://acmg.seas.harvard.edu/gamap/).

3. Results and discussions

3.1. S-ratios from experiments

At Mt. Abu, the simultaneous measurements of ambient SO_2 (Francis, 2012) and SO_4^{2-} were made during Sep '09, Oct '09, Nov '09, Dec '09, Feb '10 and Mar '10.

The molar ratio of SO_4^{2-} to total SO_x ($SO_x = SO_2 + SO_4^{2-}$), termed S-ratio, for the different sampling periods were then calculated as:

$$S-\text{ratio} = \left[SO_4^{2-}\right] / \left([SO_2] + \left[SO_4^{2-}\right]\right) \tag{1}$$

For this, the sulphate (SO_4^{2-}) in the aerosol ($PM_{2.5}$) samples were measured in the ion chromatograph. The median of the SO_2 concentrations for the corresponding sampling interval also were obtained from the time series SO_2 (Francis, 2012). The monthly median S-ratio is then calculated from the S-ratios for the different sampling intervals.

Fig. 2 shows the S-ratios for the different sampling months, and the median values are given in Table 2. During Feb '10 and Mar '10 the S-ratios were lower compared to Nov '09 and Dec '09. Intermediate between these were the values for Sep '09 and Oct '09.

The lower S-ratios for Feb '10 and Mar '10 (median values 0.10 and 0.08 respectively) may be explained by the higher PBL heights for these months and a resulting dilution of SO_2 in the lower layers of the atmosphere – to reduce the dry deposition losses of SO_2. A detailed discussion on the PBL effect on S-ratio, based on GEOS-Chem simulations, is given in Section 3.4.1. The relatively low

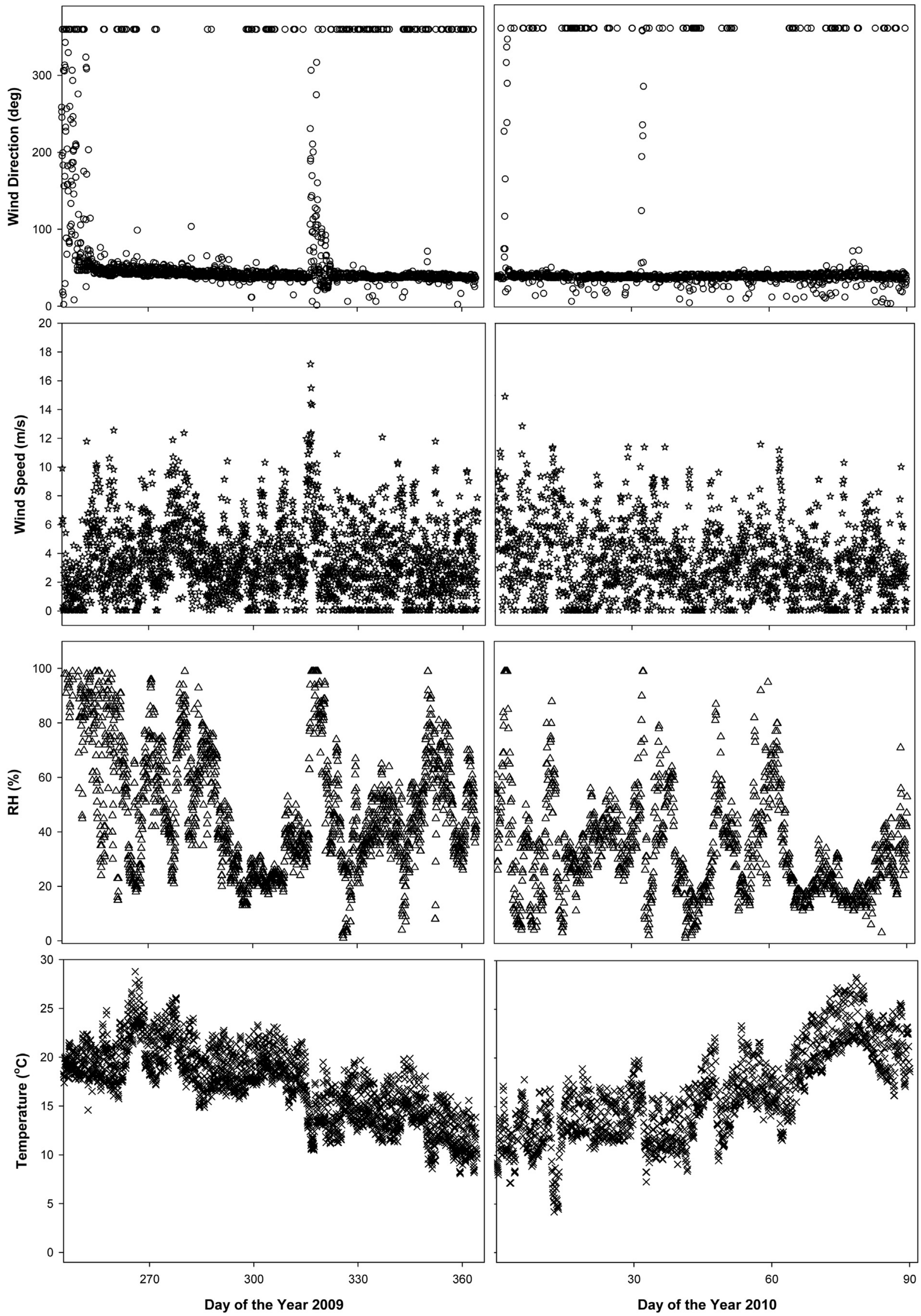

Fig. 1. Daily variation of meteorological parameters at the high altitude sampling site during September 2009 to March 2010, spanning the whole sampling months.

Table 1
Details of the Aerosol samples collected from the high altitude site (Gurushikhar, Mt. Abu), for the SO_4^{2-} measurements.

Month	Year	No. of samples collected	Sampling date (day of the year)
September	2009	17	268, 269, 270, 271, 272, 273
October	2009	16	274, 275, 276, 277, 278, 279
November	2009	23	306, 307, 308, 309, 310, 311, 312, 313, 314, 315
December	2009	30	342, 343, 350, 351, 352, 353, 354, 355, 356, 357, 358
February	2010	24	43, 44, 45, 46, 47, 48, 49, 50, 51
March	2010	43	63, 64, 65, 66, 67, 68, 69, 70, 71, 72, 73, 74, 75, 76, 77

water vapour in the atmosphere – a precursor for the OH production via photo chemistry – during Feb–Mar, is another factor for the low oxidation efficiency. The lower RH also reduces the probabilities for heterogeneous oxidation on water droplets. The lesser long range transport of SO_2 and hence a low 'aged air mass presence' (Francis, 2012) could be another important reason for low S-ratios during these months. The slightly lower S-ratio for Mar '10 (compared to Feb '10) may be explained by the higher PBL heights for Mar. Even though some favourable conditions such as higher atmospheric dust load prevail during these months – offering the possibility for heterogeneous oxidation on dust surfaces to raise S-ratios, as will be discussed in Section 3.4.2 – the effect seems to be insufficient to bring up the S-ratio values to the extent that the above negating effects are compensated. Similarly, the possibility for an enhancement in the oxidation efficiency when PBLs are high (Miyakawa et al., 2007) – for the increased atmospheric retention time of SO_2 and so an efficient oxidation to SO_4^{2-} before loss onto the surface – didn't help compensate the S-ratio decline.

The PBL heights during Nov–Dec are among the lowest of the year (Francis, 2012), leading to a higher SO_2 loss rate via dry deposition. Similarly, the long range transported SO_2 flux over Mt. Abu is among the highest during Nov and Dec (Francis, 2012), enhancing the aged air mass presence (But in this case the S-ratio needs to be interpreted with caution as it is also an indicator of air mass ageing. Also, as will be discussed in Section 3.4.4, the S-ratios during these months are significantly influenced by dry deposition). The slightly higher S-ratio for Nov '09 (0.30 (median)) compared to Dec '09 (0.28 (median)) may be explained by the higher OH levels for the former.

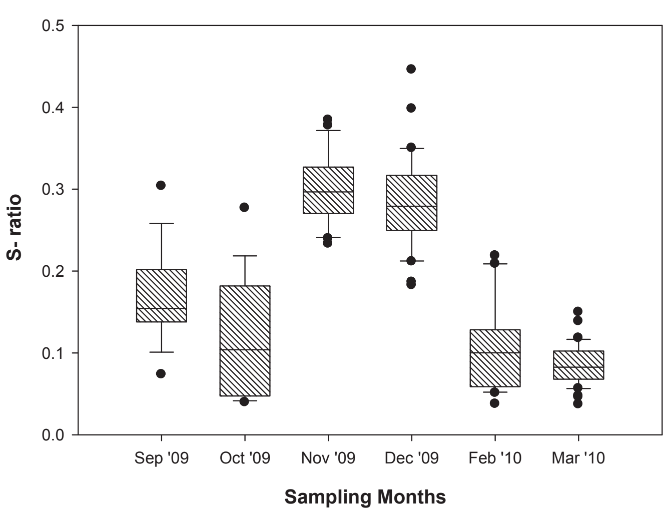

Fig. 2. Experimentally obtained S-ratios at Mt. Abu during different sampling months, showing seasonal trends. Top and bottom of the shaded box indicate 75th and 25th percentile respectively. Whiskers above and below the box indicate 90th and 10th percentile respectively. The horizontal line within the box marks the median.

During Sep '09 and Oct '09 when intermediate S-ratio values were obtained (median values 0.15 and 0.10 respectively), it is presumable the S-ratios are influenced either positively or negatively by the various parameters discussed previously such as PBL, OH, RH and long range transport – the sign and magnitude of influence decided by their relative strengths. For example, during these months, the PBL heights are lower than those for Feb and Mar, causing a more efficient removal of SO_2 via dry deposition while the SO_2 influx from long range transport is lower than that of Dec (Francis, 2012).

The PBL heights for Sep are lower than Oct to give a higher S-ratio for Sep '09 compared to the latter. Similarly the higher relative humidity for Sep is another reason for the higher S-ratio in Sep '09 compared to Oct '09.

3.2. SO_4^{2-} and SO_2 variability over Mt. Abu

In the following discussion, we presume that any in-phase variability patterns for SO_2 and SO_4^{2-} time series would suggest 'predominant local source contribution' to the measured SO_2 and SO_4^{2-} while an anti-phase suggest a 'more regionality for the sources/long range transported air mass presence', in line with the inferences from Myles et al. (2009). The various HYSPLIT (Draxler and Hess, 1998) generated 7-day airmass back trajectories employed for source apportionment in the discussions below are shown in Fig. 3.

Fig. 4a shows the SO_4^{2-} and the SO_2 (median) concentrations as well as the S-ratios for each sampling interval in Sep '09. A prominent observation for this month is that the SO_4^{2-} and SO_2 variations were in-phase with each other but with differing S-ratios. During 25th and 26th Sep '09, the SO_4^{2-} concentration and hence the S-ratios were pronounced, compared to the rest of the sampling days. This could be attributed to the aged air mass arrival from the SO_2 hot-spot region surrounding 30° N, 75° E (Francis, 2012), as evidenced by the HYSPLIT trajectories.

Similarly, during Oct '09, the SO_4^{2-} and SO_2 (median) variabilities were in-phase (Fig. 4b). The SO_4^{2-} as well as the S-ratios enhanced during the initial days (1st, 2nd and 3rd (till 01.29 h IST) Oct '09) which could be attributed to the aged air mass arrival from the SO_2 hot-spot region surrounding 30° N, 75° E, as evidenced by the HYSPLIT trajectories. The SO_4^{2-} and the S-ratios were lower during 3rd (from 10.33 h IST), 4th, and 5th (till 10.26 h IST)

Table 2
The median S-ratio values over Mt. Abu for the different sampling months, calculated from the field measurements of SO_4^{2-} and SO_2.

Sampling month	Year	S-ratio (median)
September	2009	0.15
October	2009	0.10
November	2009	0.30
December	2009	0.28
February	2010	0.10
March	2010	0.08

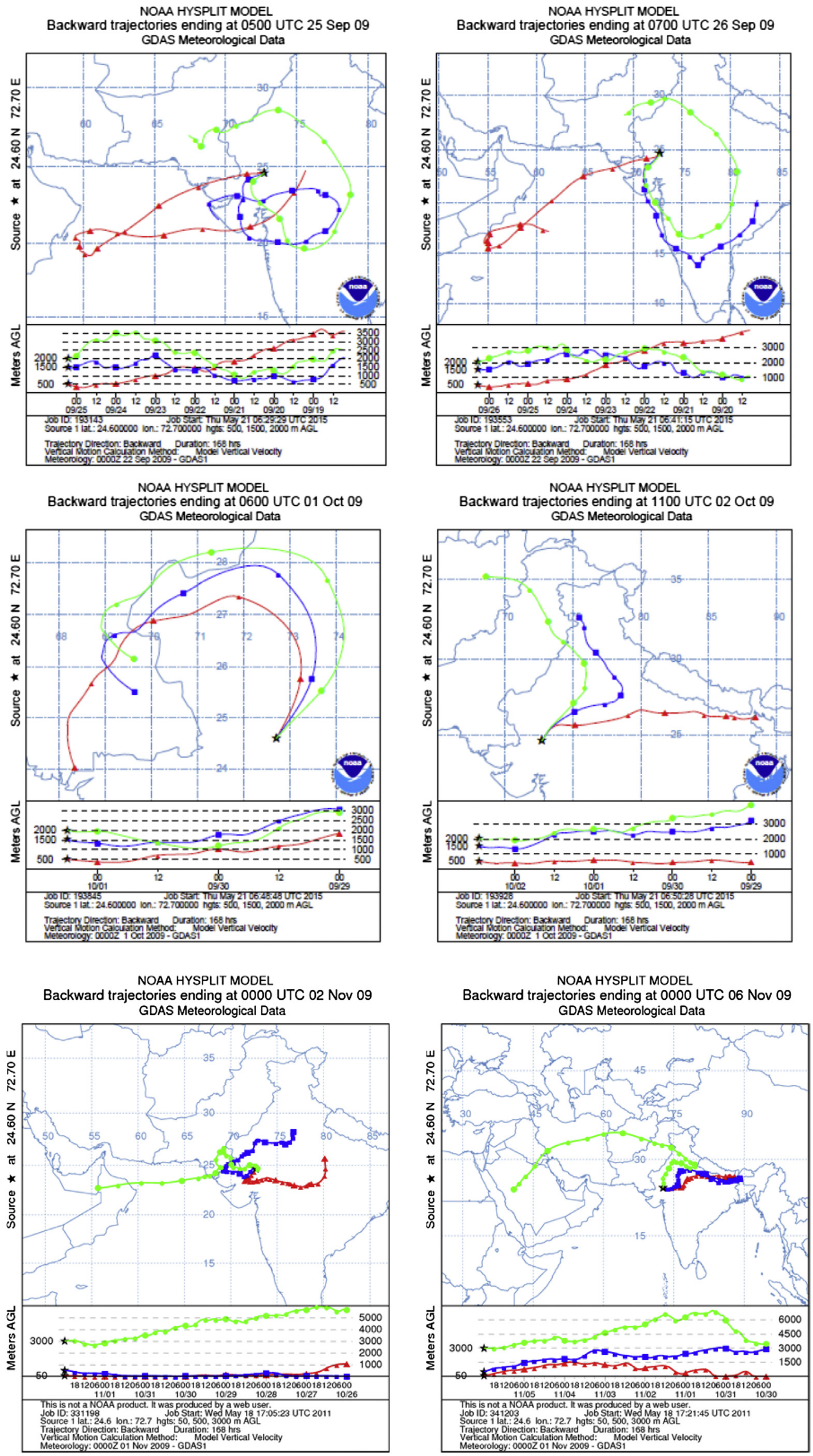

Fig. 3. HYSPLIT 7-day airmass back trajectories during relevant days, for sampling periods spanning Sep–Dec 2009 and Feb–Mar 2010.

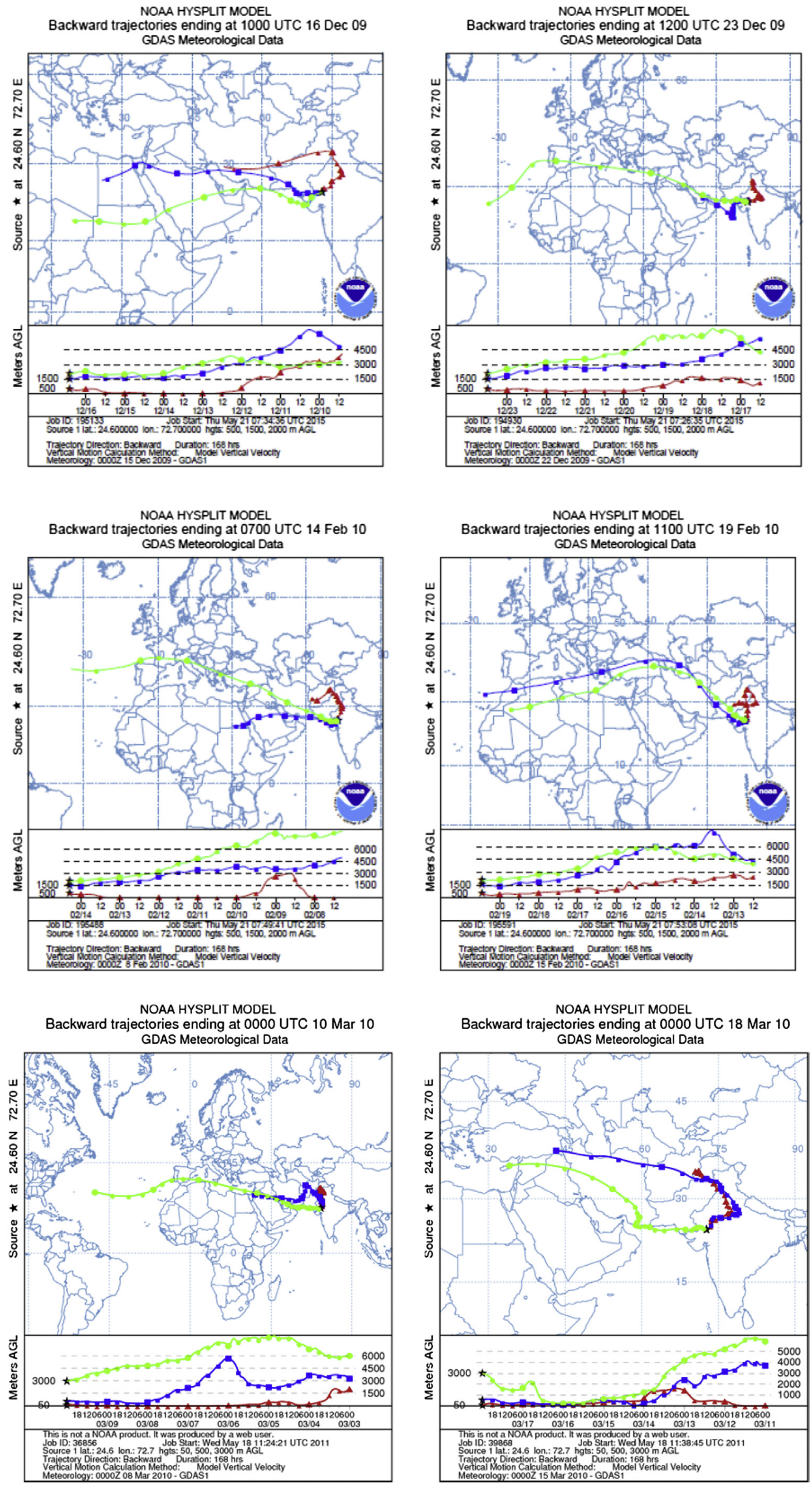

Fig. 3. Continued

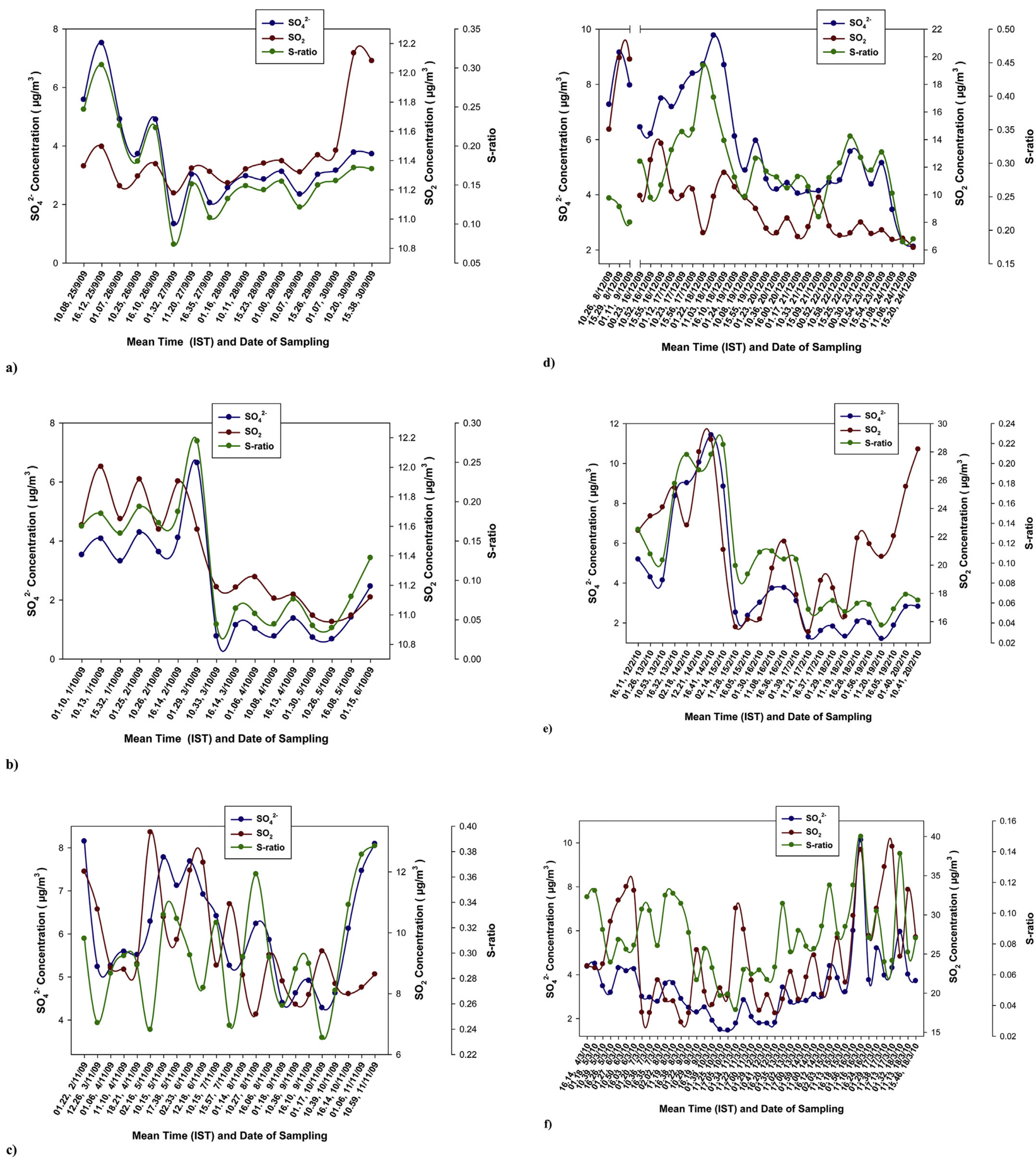

Fig. 4. The SO_4^{2-} and SO_2 (median) concentrations as well as S-ratios at Mt. Abu during each sampling interval (mean time in Hrs shown along X-axis) for: a) September 2009, b) October 2009, c) November 2009, d) December 2009, e) February 2010, and f) March 2010.

Oct '09, when the back-trajectories extended to low SO_2 regions in the eastern side of the sampling site.

In Nov '09, when major SO_2 plume transports from an oil fire event – burning nearly 60,000 kL of oil – at a nearby location, Jaipur (26.92° N, 75.82° E), were reported (Francis, 2012), the SO_4^{2-} and SO_2 (median) peaks (Fig. 4c) were in-phase during the initial days which moved out-of-phase by the second half of the sampling period. This may be explained as follows. The huge oil fire released large amounts of SO_2 to the ambient atmosphere. As the plume is transported, there exist various pathways deciding the SO_2 levels reaching the high altitude sampling site: (i) oxidation of the SO_2 to SO_4^{2-} as the plume transport downwind, (ii) dilution of the plume with air containing sulphur present as SO_4^{2-} or (iii) a combination of these two processes. During the initial days, the SO_2 got transported predominantly compared to SO_4^{2-}, for the former's higher concentrations in the oil fire plume. This SO_2 after reaching the sampling site undergo oxidation locally to give an in-phase varying SO_2-SO_4^{2-}. Similarly, the high pollutant levels could have caused a depletion of OH radicals over the oil fire site, reducing the atmospheric oxidation efficiency locally and hence a low SO_4^{2-}, over the oil fire site. By the second half of the sampling period when the plume dilute with background air, the atmosphere start replenishing OH and hence its oxidation power, to result in enhanced SO_4^{2-} production. This would result in SO_4^{2-} rich air parcels reaching the sampling site by the second half of the sampling period, when the SO_2 emissions almost ceased as the fire exhausted. This mechanism explains the observed anti-phase during the second half of the sampling period. The arguments are supported with the back trajectory analysis.

In Dec '09, the SO_4^{2-} – SO_2 (median) peaks showed least agreement in phase and magnitude (Fig. 4d). This could be attributed to the enhanced long range transported SO_2 air masses for this month (Francis, 2012). When air masses are transported over longer distances, the SO_2 and SO_4^{2-} is expected to show poor correlation, for their varying loss mechanisms and mobility patterns. Higher altitude back trajectories (1500 m and 2000 m AGL) for this month extend to the SO_2 hot spot region in Middle East – significant industrial activity exists along the NE Saudi coast between Bahrain and Kuwait, and some of these industries (e.g., gas desulfurization plants) emit substantial quantities of SO_2 (Daum et al., 1993) as seen in the GEOS-Chem generated profiles for the region (Francis, 2011) – while lower level trajectories (500 m AGL) extend to the SO_2 hot-spot region surrounding 30° N, 75° E. The observations of 'poor SO_2-SO_4^{2-} correlations in long range transported air masses' have the scope for further systematic simulation/field studies on the topic.

During Feb '10, the SO_4^{2-} and SO_2 (median) variabilities (Fig. 4e) were in-phase with each other but with differing S-ratio values – which were pronounced during the initial sampling days. Again in Mar '10, the SO_4^{2-} and SO_2 (median) variabilities (Fig. 4f) were more or less in-phase with only a few exceptions – towards the end of the sampling period, when high intensity SO_2 spikes were present, the SO_4^{2-} peaks went out of phase with those of SO_2.

3.3. S-ratios from GEOS-Chem: comparing with observations

Fig. 5 shows the S-ratios from GEOS-Chem model for different months of the year 2009, for the GEOS-Chem 4° × 5° grid cell containing the sampling site. For this the time series SO_2 and SO_4^{2-} were generated (every 2-h) by turning on the ND49 diagnostics in the 'input.geos' file, and the S-ratios were calculated using Eq. (1). The model generated S-ratios showed a pronounced seasonality with the highest ratios during Jul–Aug, and the lowest in Apr. The diurnal variability patterns for the S-ratios and its seasonal trends are elaborated in the Supplementary material.

Having calculated the S-ratios from both observations and the model, it would be inevitable to compare the two. But, such a comparison will be limited by the following factors: (a) While the model calculations for each month spans whole days of the month, the observational data covers only a few days per month, (b) The model results are for the ground level, while the sampling site is located at a higher altitude, (c) Inter-annual variabilities could be influencing the comparisons – the model simulations are for year 2009, while the observations spans 2009 and 2010, (d) Single point measurements are compared with the grid-averaged values from a coarse resolution (4° × 5°) model run.

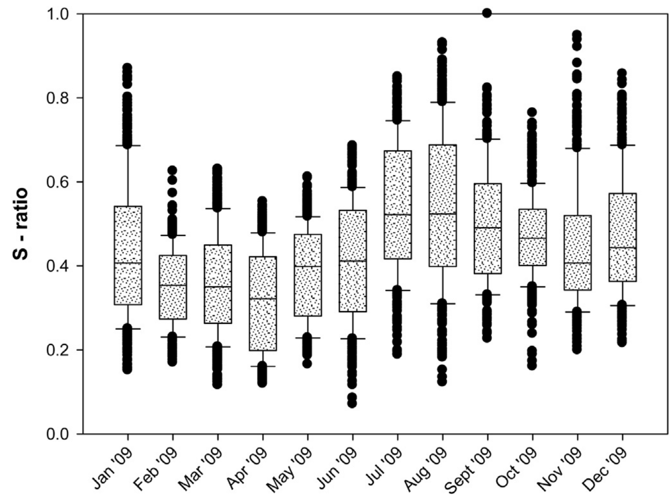

Fig. 5. S-ratios calculated from the model runs, for the GEOS-Chem 4° × 5° grid cell containing the sampling site. Top and bottom of the shaded box indicate 75th and 25th percentile respectively. Whiskers above and below the box indicate 90th and 10th percentile respectively. The horizontal line within the box marks the median.

Despite these shortfalls, the model appears to have captured some of the trends in the S-ratios from field measurements. For example, the S-ratios for Feb–Mar are lower than those for Sep–Oct in both observations and model. Similarly the model prediction that the monthly median S-ratio for Sep is higher than that for Oct, is seen to hold true in the observations too. On the other hand, the model results for Nov–Dec deviate significantly from the observations. While the model predicts Nov–Dec S-ratios to be lower than that of Sep–Oct and higher than Feb–Mar, the observations showed Nov–Dec with higher S-ratios, compared to the rest. This could be explained based on the discussions in Section 3.5 – where the S-ratios are shown to increase with altitude, for Dec – and clubbing it with the shortfall (b), mentioned above – viz, the model results are at a lower altitude compared to the observations – explain the observed discrepancy for Dec. With the meteorological conditions for Nov closely resembling Dec, similar arguments could be applied to Nov. Also, part of the discrepancies for Nov can result from the absence of the accidental oil fire emissions (in Jaipur: 26.92° N, 75.82° E) inventory in the model runs. As discussed in Section 3.2, the anomalous SO_2 – SO_4^{2-} variability patterns in the field measurements during Nov '09 were linked to the plume transports from the oil fire site - which is missing in the model runs.

Another prominent deviation is in the magnitudes of the monthly median S-ratios – the model values are higher than the observations throughout the different sampling months, though with varying strengths. This could be linked to a known problem with the GEOS-5 meteorology fields, which suffer from an artificially low mixed layer depth at nighttime, as is discussed in Section 3.4.1. Also, earlier studies (Drury et al., 2010) have shown a model bias in GEOS-Chem generated sulphate concentrations. They found that the model sulphate masses were 50–100% higher than the observations. The bias was mainly in the strong aerosol source regions of the Midwest and mid-Atlantic; and minimal bias outside these source regions. They suggested that the model sulphate bias is likely caused by an overestimate of the rate of SO_2 oxidation. McKeen et al. (2007) found that regional models omitting aqueous-phase SO_2 oxidation in clouds did not overestimate the measured sulphate. This lack of bias found by McKeen et al. (2007) for the regional models incorporating only gas-phase oxidation of SO_2 suggests that models in general may be overestimating the contribution to sulphate from aqueous-phase SO_2 oxidation in clouds, and hence to an overestimation of the S-ratios.

3.4. Influence of various parameters/processes on S-ratio

The seasonal variation in S-ratio is presumably dictated by the seasonality in the atmospheric parameters influencing the SO_2 oxidation and/or the seasonality in the sources and sinks of SO_2 and SO_4^{2-}.

In Section 3.4.1, the S-ratio modulations by OH and PBL are discussed and its seasonal trends are analysed. The sensitivity simulations discussed in Sections 3.4.2–3.4.4 assess the effect of switching off different atmospheric processes – dust emission, transport, dry deposition – on the S-ratios, via the equation:

$$\Delta S_{process} = \left(S' - S\right)/S \times 100\% \tag{2}$$

where:

$\Delta S_{process}$ = Percent Difference in S-ratio in the absence of the 'Process'

S = S-ratios calculated from the baseline run employing the standard input.geos file

S′ = S-ratio calculated from the sensitivity run with the particular 'process' turned OFF

3.4.1. S-ratio dependence on OH and PBL

The time series OH concentrations and PBL heights (every 2-h) for the GEOS-Chem 4° × 5° grid cell containing the sampling site for year 2009, generated via turning ON the ND49 diagnostics, are elaborated in Francis (2012). Fig. 6 shows colour coded 2D scatter plots with S-ratios as function of OH radical and PBL height. The S-ratio values are represented as a colour bar.

It has been recently reported (Heald et al., 2012; Walker et al., 2012) that the GEOS-5 meteorology fields suffer from an artificially low mixed layer depth at nighttime which can produce large biases in simulated nighttime surface concentrations of various species. They attempted to correct this problem by restricting the mixed layer depth from dropping below a minimum mechanical mixing depth, defined as a function of local friction velocity. It may be noted that, in the present study such a correction is not undertaken and could possibly cause a bias in the model generated SO_2 and SO_4^{2-} concentrations and hence the S-ratios.

In Jan, the S-ratios show many non-systematic peaks (i.e. the peaks which do not vary systematically with PBL and OH) - suggestive of transient long range transport of aged air masses. In Feb, the non-systematic peaks almost vanished, indicating the prominent roles by PBL and OH in deciding the S-ratio. For this month, the S-ratios were more or less constant for OH greater than ~5e + 5 and PBL higher than ~1100 m. In Mar, for OH greater than ~2e + 6, the S-ratio values seem to increase with PBL height, supporting the arguments of Miyakawa et al. (2007) – a higher boundary layer for summer results in enhanced retention time for SO_2 which in turn cause an efficient oxidation to SO_4^{2-} before loss onto the surface. In Apr, the PBL maximum reached ~4000 m, but the OH remained similar to Mar and the monthly median S-ratio gave the lowest value of the year. During May, when the monthly S-ratio switched to ascending mode, the PBL maximum reached ~4500 m and the OH maximum was ~1e + 7. In this month, for OH greater than ~1e + 6 the S-ratios are low for PBL below ~500 m, while the ratios enhance for PBL above ~2500 m. In Jun, above an OH of ~5e + 6, the S-ratios were enhanced for most PBL heights. Many non-systematic peaks (medium intensity) are observed for this month – attributed to heterogeneous oxidation pathways, for the occasional rise in RH. In Jul, the PBL maximum was just ~2500 m and OH levels were among the highest of the year. For this month, the S-ratio peaks (high intensity) are seen for OH greater than ~1e + 6 and PBL below ~1500 m. The higher RH and hence the possible heterogeneous oxidation pathways is another major reason for the higher S-ratios for this month, as evidenced by many non-systematic peaks. In Aug, the PBL maximum was just ~1500 m – the lowest of the year – and OH maximum was ~2e + 7. A combination of low PBL, high OH – for the possible enhanced entrainment of moist air - along with heterogeneous oxidation pathways, helps this month record the highest S-ratio of the year. In Sep, when the PBL increased above Aug and OH levels decreased, the S-ratio also declined. Non-systematic peaks were observed for this month, attributed to the transient aged air mass influx and/or to transient fluctuations in RH. In Oct, when the monthly median S-ratio declined further, the PBL enhanced and the OH decreased below the previous month. A few non-systematic peaks (medium intensity) were noted in this month. In Nov, many non-systematic S-ratio peaks is a prominent feature, attributed to the aged air mass arrivals. In Dec, when the monthly median S-ratio switched to the ascending phase, the PBL decreased below Nov. Similar to Jan and Nov, many non-systematic S-ratio peaks are observed for this month, which are due to the significant long range transported (hence aged) SO_2 air parcel influx during this month (Francis, 2012).

In a similar fashion, elaborate discussions on the S-ratio modulations by OH and RH and their seasonal trends are given in the Supplementary material.

3.4.2. Effect of atmospheric dust load on S-ratio

Reactions with mineral particles influence sulphur budgets downwind of major dust source regions (Dentener et al., 1996; Li-Jones and Prospero, 1998; Zhang and Carmichael, 1999). To assess such effects to the S-ratios, over this semi-arid region with a high abundance of mineral dust (Kumar and Sarin, 2009, 2010), sensitivity simulations were performed with dust emissions turned OFF. The 'percent difference in S-ratio in the absence of dust emission ($\Delta S_{DustEmission}$)', for the GEOS-Chem 4° × 5° grid containing the sampling site, is then obtained via the Eq. (2). Here, the 'process' in the equation is 'Dust Emission'.

Fig. 7a shows the seasonal patterns in the $\Delta S_{DustEmission}$. In the absence of dust emission, the S-ratios decreased below their values for the baseline run. The $\Delta S_{DustEmission}$ is among the lowest during Feb, Mar, Apr and May (when the dust load over the region build up) with peak reduction (~4.7% (median)) in May – the month having the highest atmospheric dust load.

3.4.3. Effect of transport on S-ratio

To study the effect of transport, sensitivity simulations were performed with transport turned OFF. The 'percent difference in S-ratio in the absence of transport ($\Delta S_{Transport}$)', is then obtained via the Eq. (2). Here, the 'process' in the equation is 'Transport'. The $\Delta S_{Transport}$ showed a seasonal variability (Fig. 7b). During Dec, Jan, Feb, Mar, April and May, the S-ratios enhanced in the absence of transport, above its value for baseline runs, with highest value in April. Near-zero/slightly negative values for $\Delta S_{Transport}$ were obtained during Jul, Aug, Sep and Oct.

These patterns may be explained by the model predictions in Francis (2012), wherein 'switching off the transport' is shown to cause a reduction in the SO_2 levels in the grid cell containing the Mt. Abu region, throughout the year – suggesting that the SO_2 emissions within this grid cell are lower than those in the upwind grid cells. Further, the study showed that the months Jan, Feb, Mar and Apr receive the minimum SO_2 contribution from long range transport, while Jul and Dec sees the highest contribution. As discussed in Section 3.3, during Dec, Jan, Feb, Mar, April and May, the S-ratios and hence the SO_2 oxidation rates are poor over the region. So an enhanced influx of SO_2 via transport during these months doesn't enhance SO_4^{2-} formation significantly, but lead to a reduction in the S-ratios, for the increased SO_2 levels. On the other hand, during Jul, Aug, Sep and Oct, favourable conditions prevail for an efficient SO_2 oxidation. This implies that, during these months, any additional supply of SO_2 will be efficiently converted

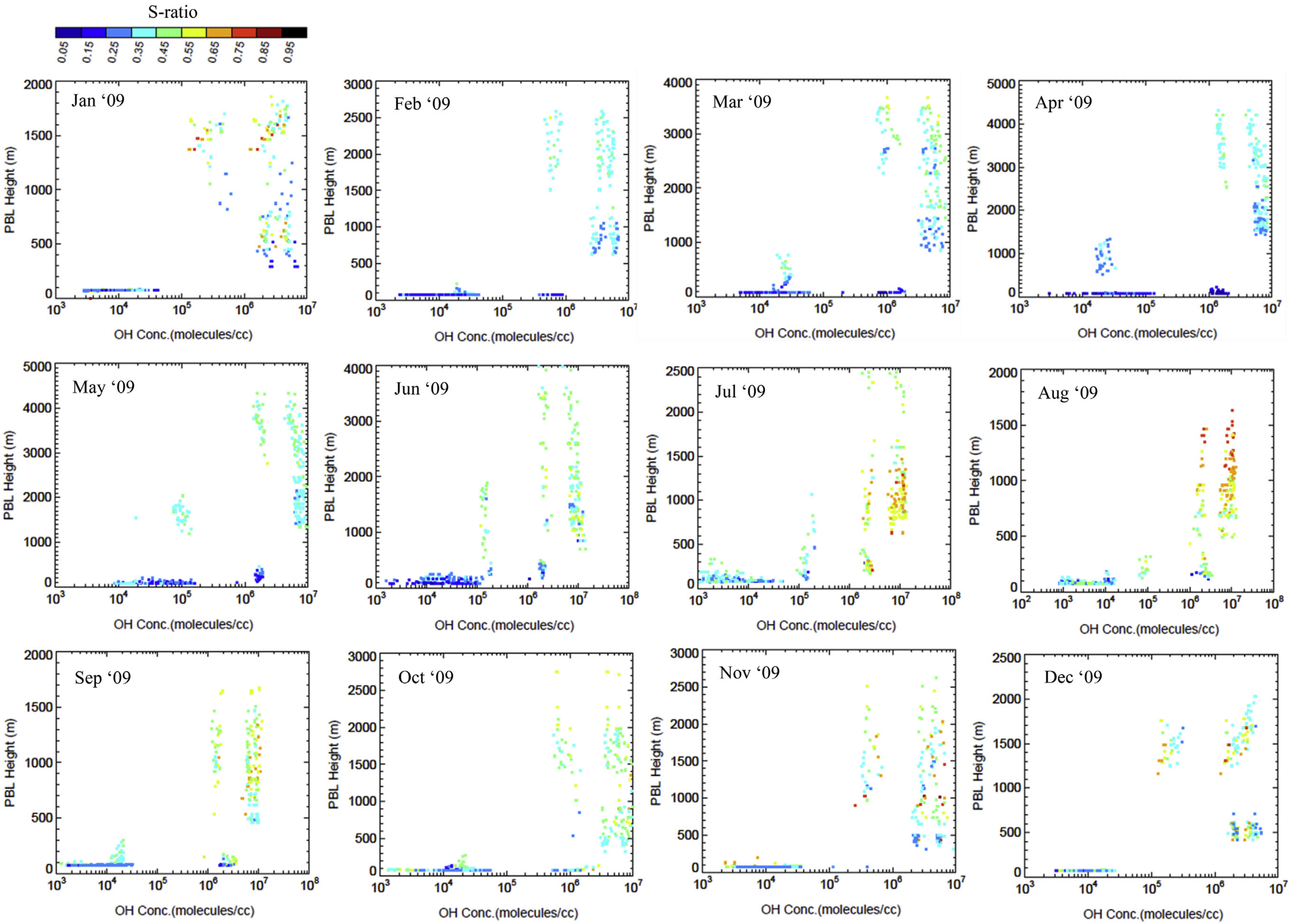

Fig. 6. Plots showing the S-ratio dependence on the OH radical concentration (molecules/cc) and PBL height (m), for the GEOS-Chem 4° × 5° grid cell containing the sampling site.

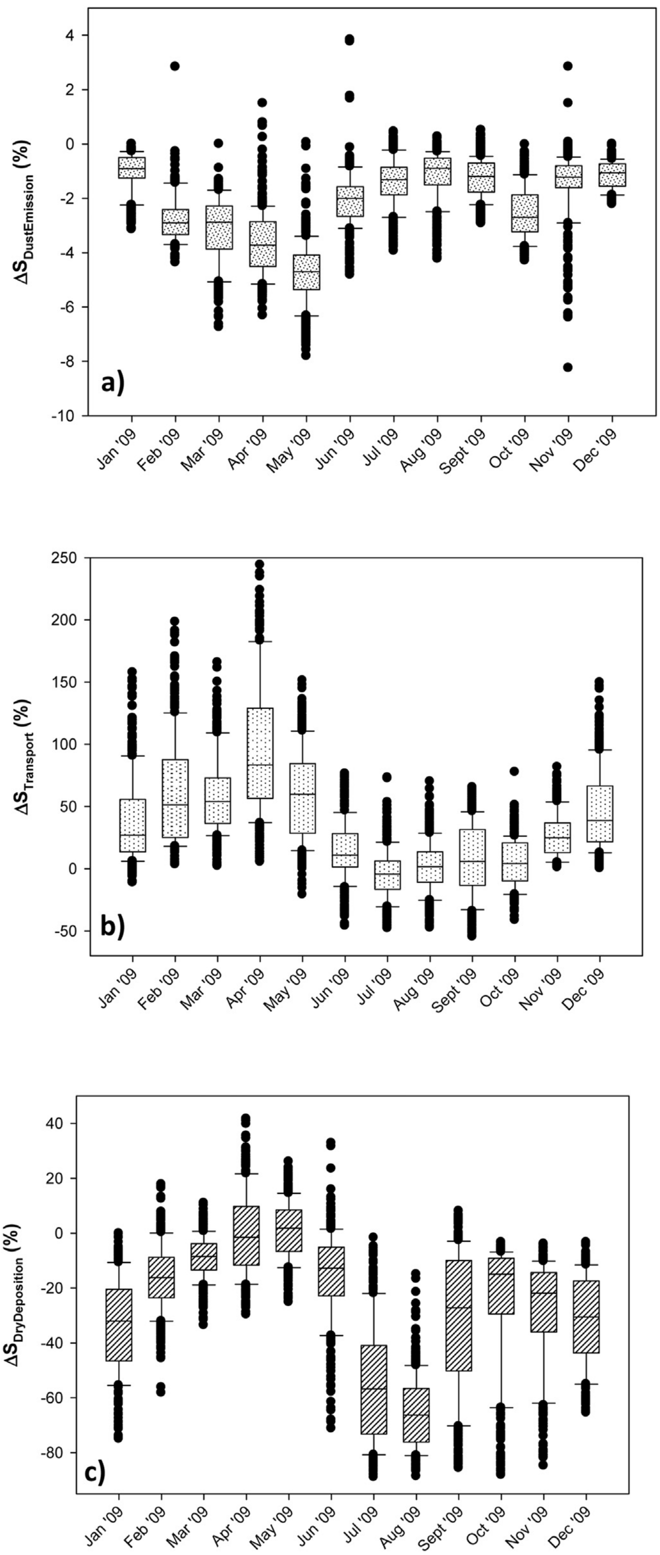

Fig. 7. (a) $\Delta S_{DustEmission}$, b) $\Delta S_{Transport}$ and c) $\Delta S_{DryDeposition}$, obtained via sensitivity simulations, for the GEOS-Chem 4° × 5° grid cell containing the sampling site. Top and bottom of the shaded box indicate 75th and 25th percentile respectively. Whiskers above and below the box indicate 90th and 10th percentile respectively. The horizontal line within the box marks the median.

to SO_4^{2-} to lead to a stable/slightly higher S-ratios when the 'transport is ON'.

3.4.4. Effect of dry deposition on S-ratio

Dry deposition plays prominent roles in the removal process of air pollutants from the atmosphere (Erisman et al., 2005; Gupta et al., 2004; Lee and Lee, 2004; Edwards et al., 1999; Yi et al., 1997; Bidleman, 1988; Zeller et al., 1997; Raymond et al., 2004). To assess the effects of seasonal fluctuations in the dry deposition, on the S-ratios, sensitivity simulations were performed with dry deposition OFF. The 'percent difference in S-ratio in the absence of dry deposition ($\Delta S_{DryDeposition}$) ', is then obtained via the Eq. (2). Here, the 'process' in the equation is 'Dry Deposition'.

Fig. 7c shows the $\Delta S_{DryDeposition}$ for different months of the year 2009. In the absence of dry deposition, the S-ratios decreased below their values for baseline run. This could be attributed to the preferential dry deposition loss of SO_2 compared to SO_4^{2-}. The $\Delta S_{DryDeposition}$ is lowest in Aug (~66.3% (median) reduction) followed by Jul. The $\Delta S_{DryDeposition}$ is high (less negative) during Mar, Apr and May with the highest value in May, which may be explained as follows. During these months the PBL is among the highest to have a lesser amount of SO_2 and SO_4^{2-} in the lower layers of the atmosphere – thus reduce the loss via dry deposition.

3.5. Altitudinal dependence of S-ratio

To study the altitudinal dependence, S-ratios at various altitudes were derived from the model, for the months May, Jul, and Dec 2009, in the GEOS-Chem 4° × 5° grid cell containing the sampling site.

During May '09, – a summer (pre-monsoon) month when the PBL reach the highest value of the year (Francis, 2012) – the S-ratios (Fig. 8a) increased slightly with altitude till 0.9 km AGL, which then remained almost constant till 4.2 km AGL. This may be explained as follows. The high PBL heights for the month ensure that the altitudes considered here are within the PBL during most of the time, with least probabilities for experiencing free-tropospheric conditions. This allows for well-mixing of the SO_2 and SO_4^{2-}, resulting in the uniform S-ratio patterns till about 4.2 km AGL. The spread in S-ratio values was highest at the ground, which may be attributed to the air turbulence and the associated variations in transport/loss mechanisms at the ground level, to lead to non-uniform oxidation/loss rates for SO_2.

Fig. 8b shows the altitudinal variation in S-ratios for Jul '09 – a monsoon month when the RH is high and the OH concentration is the highest of the year (Francis, 2012). The S-ratios increased in magnitude till 3 km AGL from where it remained more or less constant till 4.2 km AGL. The increase in S-ratios till 3 km AGL could be attributed to the enhanced cloud water presence at the higher altitudes, and hence the heterogeneous oxidation pathways. For this month, the S-ratio spread was high throughout the different altitudes, compared to May '09.

For Dec '09 – a winter month, when the OH radical concentration is the lowest of the year (Francis, 2012) – the altitudinal variation in the S-ratios showed features (Fig. 8c) different from the other two months. After a slight increase in the S-ratios from 0.3 km to 0.6 km AGL, the ratios remained steady till 2.7 km AGL, followed by a steep increase. This could be explained as follows. Since the PBL heights for the region are very low in December, free tropospheric conditions prevail above an altitude of 2.7 km AGL. The long range transport of SO_2 peak during December (Francis, 2012) over the sampling region. This aged air mass transport, occurring at free tropospheric altitudes, bring air parcels with enhanced SO_4^{2-} content, causing S-ratio increase with altitude above 3 km AGL. The spread in S-ratio values for this month is high throughout the different altitudes, compared to May '09 and Jul

'09, and is attributed to the non-systematic patterns in the long range transport of aged air masses.

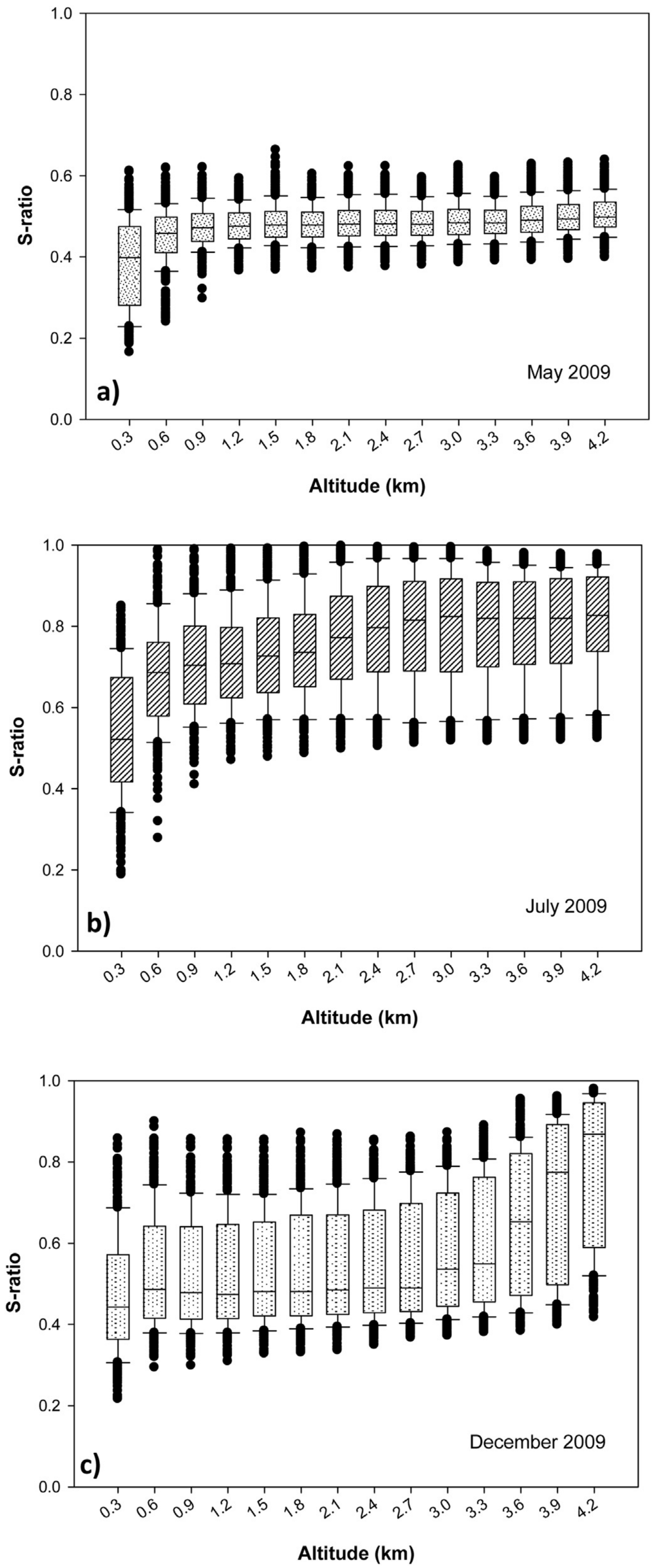

Fig. 8. Variability in S-ratios as function of altitude above ground level for, a) May 2009, b) July 2009, and c) December 2009, for the GEOS-Chem 4° × 5° grid cell containing the sampling site. Top and bottom of the shaded box indicate 75th and 25th percentile respectively. Whiskers above and below the box indicate 90th and 10th percentile respectively. The horizontal line within the box marks the median.

4. Conclusions

The molar ratio of SO_4^{2-} to total SO_x ($SO_x = SO_2 + SO_4^{2-}$), termed S-ratio, derived from field measurements at the high altitude site showed a pronounced seasonality. During Feb–Mar '10 the S-ratios were lower compared to Nov–Dec '09 and intermediate ratios were obtained in Sep–Oct '09. The lower ratios for Feb–Mar '10 have been attributed to the higher PBL heights – to reduce the dry deposition losses of SO_2 – as well as the lower OH and RH levels for these months. The relatively low PBL heights and pronounced 'aged air mass presence' (Francis, 2012) are projected as the possible factors for the higher S-ratios in Nov–Dec '09.

The SO_4^{2-} and SO_2 variations were in-phase with each other during Sep–Oct '09 and Feb–Mar '10, while the agreement was poor during Dec '09. In Nov '09, the in-phase variabilities prevailed during the initial days which then moved out-of-phase by the second half. The in-phase variability patterns are presumed to suggest 'predominant local source contribution' to the measured SO_2 and SO_4^{2-} while an anti-phase suggests a 'more regionality for the sources/long range transported air mass presence'.

S-ratios from the model runs exhibited a pronounced seasonality with the highest ratios in Jul–Aug and the lowest in Apr. The contributions from various parameters such as PBL, OH, RH, dust load, transport pattern and dry deposition also were assessed via the model. Sensitivity simulations showed the S-ratios enhancing due to 'dust emission' with the peak (~4.7%, median value) in May. The 'transport' is seen to reduce the S-ratios during Dec, Jan, Feb, Mar, April, May while enhance it during Jul, Aug, Sep, Oct. Similarly, the 'dry deposition' boosts the S-ratios with the peak in Aug (~66.3%, median value). The altitudinal dependence of S-ratios studied via the CTM, indicated a seasonality in its behaviour.

Acknowledgements

The ISRO-Geosphere Biosphere Program (Department of Space, Government of India) is gratefully acknowledged for the partial financial support for this study. We thank the two anonymous reviewers and the editor for their constructive comments.

Appendix A. Supplementary data

Supplementary data related to this article can be found at http://dx.doi.org/10.1016/j.atmosenv.2015.09.021.

References

Alexander, B., Savarino, J., Lee, C.C.W., Park, R.J., Jacob, D.J., Thiemens, M.H., Li, Q.B., Yantosca, R.M., 2005. Sulfate formation in sea-salt aerosols: constraints from oxygen isotopes. J. Geophys. Res. 110, D10307.
Bey, I., Jacob, D.J., Yantosca, R.M., Logan, J.A., Field, B.D., Fiore, A.M., Li, Q., Liu, H.Y., Mickley, L.J., Schultz, M.G., 2001. Global modeling of tropospheric chemistry with assimilated meteorology: model description and evaluation. J. Geophys. Res. 106 (D19), 23073–23095.
Bidleman, T.F., 1988. Atmospheric processes: wet and dry deposition of organic compounds are controlled by their vapor-particle partitioning. Environ. Sci. Technol. 22, 361–367.
Chen, D., Wang, Y., McElroy, M.B., He, K., Yantosca, R.M., Le Sager, P., 2009. Regional CO pollution and export in China simulated by the high-resolution nested-grid GEOS-Chem model. Atmos. Chem. Phys. 9 (11), 3825–3839.
Daum, P.H., Al-Sunaid, A., Busness, K.M., Hales, J.M., Mazurek, M., 1993. Studies of the Kuwait oil fire plume during midsummer 1991. J. Geophys. Res. 98, 16,809–16,827.
Dentener, F.J., Carmichael, G.R., Zhang, Y., Lelieveld, J., Crutzen, P.J., 1996. Role of mineral aerosol as a reactive surface in the global troposphere. J. Geophys. Res. 101 (D17), 22869–22889.
Draxler, R.R., Hess, G.D., 1998. An overview of the HYSPLIT_4 modeling system of trajectories, dispersion, and deposition. Aust. Meteorol. Mag. 47, 295–308.

Drury, E., Jacob, D.J., Spurr, R.J.D., Wang, J., Shinozuka, Y., Anderson, B.E., Clarke, A.D., Dibb, J., McNaughton, C., Weber, R., 2010. Synthesis of satellite (MODIS), aircraft (ICARTT), and surface (IMPROVE, EPA-AQS, AERONET) aerosol observations over eastern North America to improve MODIS aerosol retrievals and constrain surface aerosol concentrations and sources. J. Geophys. Res. 115, D14204. http://dx.doi.org/10.1029/2009JD012629.
Edwards, P.J., Gregory, J.D., Allen, H.L., 1999. Seasonal sulfate deposition and export patterns for a small Appalachian watershed. Water Air Soil Pollut. 110, 137–155.
EPA I, 1996. Air Quality Criteria for Particulate Matter EPA/600/P-95/001aF. Office of Research and Development, Research Triangle Park, NC.
EPA II, 1996. Air Quality Criteria for Particulate Matter EPA/600/P-95/001bF. Office of Research and Development, Research Triangle Park, NC 11:76–11:96.
Erisman, J.W., Vermeulen, A., Hensen, A., Flechard, C., Dammgen, U., Fowler, D., Sutton, M., Grunhage, L., Tuovinen, J.-P., 2005. Monitoring and modelling of biosphere/atmosphere exchange of gases and aerosols in Europe. Environ. Pollut. 133, 403–413.
Fairlie, T.D., Jacob, D.J., Park, R.J., 2007. The impact of transpacific transport of mineral dust in the United States. Atmos. Environ. 41 (6), 1251–1266.
Francis, T., 2011. Effect of Asian dust storms on the ambient SO_2 concentration over North-East India: a case study. J. Environ. Prot. 2 (6), 778–795. http://dx.doi.org/10.4236/jep.2011.26090.
Francis, T., 2012. Temporal trends in ambient SO_2 at a high altitude site in semi-arid western India: observations versus chemical transport modeling. J. Environ. Prot. 3 (7), 657–680. http://dx.doi.org/10.4236/jep.2012.37079.
Gupta, A., Kumar, R., Kumari, K.M., Srivastava, S.S., 2004. Atmospheric dry deposition to leaf surfaces at a rural site of India. Chemosphere 55, 1097–1107.
Heald, C.L., Collett Jr., J.L., Lee, T., Benedict, K.B., Schwandner, F.M., Li, Y., Clarisse, L., Hurtmans, D.R., Van Damme, M., Clerbaux, C., Coheur, P.-F., Philip, S., Martin, R.V., Pye, H.O.T., 2012. Atmospheric ammonia and particulate inorganic nitrogen over the United States. Atmos. Chem. Phys. 12, 10295–10312. http://dx.doi.org/10.5194/acp-12-10295-2012.
Hidy, G.M., Mueller, P.K., Tong, E.Y., 1978. Spatial and temporal distributions of airborne sulfate in parts of the United States. Atmos. Environ. 12 (1–3), 735–752.
Husar, R.B., Patterson, D.E., 1980. Regional scale air pollution: sources and effects. Ann. N. Y. Acad. Sci. 338, 399–417. http://dx.doi.org/10.1111/j.1749-6632.1980.tb17136.x.
Igarashi, Y., Sawa, Y., Yoshioka, K., Matsueda, H., Fujii, K., Dokiya, Y., 2004. Monitoring the SO_2 concentration at the summit of Mt. Fuji and a comparison with other trace gases during winter. J. Geophys. Res. 109, D17304. http://dx.doi.org/10.1029/2003JD004428.
Kaneyasu, N., Ohta, S., Murao, N., 1995. Seasonal variation in the chemical composition of atmospheric aerosols and gaseous species in Sapporo, Japan. Atmos. Environ. 29 (13), 1559–1568.
Kuhns, H., Green, M., Etyemezian, V., 2003. Big Bend Regional Aerosol and Visibility Observational (BRAVO) Study Emissions Inventory. Desert Research Institute, Las Vegas, Nevada.
Kumar, A., Sarin, M.M., 2009. Mineral aerosols from western India: temporal variability of coarse and fine atmospheric dust and elemental characteristics. Atmos. Environ. 43 (26), 4005–4013.
Kumar, A., Sarin, M.M., 2010. Atmospheric water-soluble constituents in fine and coarse mode aerosols from high-altitude site in western India: long-range transport and seasonal variability. Atmos. Environ. 44 (10), 1245–1254.
Lee, B.-K., Lee, C.-B., 2004. Development of an improved dry and wet deposition collector and the atmospheric deposition of PAHs onto Ulsan Bay, Korea. Atmos. Environ. 38, 863–871.
Levy, H., 1971. Normal atmosphere: large radical and formaldehyde concentrations predicted. Science 173, 141–143.
Li-Jones, X., Prospero, J.M., 1998. Variations in the size distribution of non-sea-salt sulfate aerosol in the marine boundary layer at Barbados: impact of African dust. J. Geophys. Res. 103 (D13), 16073–16084.
Liu, H.Y., Jacob, D.J., Bey, I., Yantosca, R.M., 2001. Constraints from Pb-210 and Be-7 on wet deposition and transport in a global three-dimensional chemical tracer model driven by assimilated meteorological fields. J. Geophys. Res. 106, 12109–12128.
Luke, W.T., 1997. Evaluation of a commercial pulsed fluorescence detector for the measurement of low-level SO_2 concentrations during the gas-phase sulfur intercomparison experiment. J. Geophys. Res. 102, 16255–16265. http://dx.doi.org/10.1029/96JD03347.
Luria, M., Boatman, J.F., Harris, J., Ray, J., Straube, T., Chin, J., Gunter, R.L., Herbert, G., Gerlach, T.M., Van Valin, C.C., 1992. Atmospheric sulfur dioxide at Mauna Loa, Hawaii. J. Geophys. Res. 97, 6011–6022. http://dx.doi.org/10.1029/91JD03126.
McKeen, S., Chung, S.H., Wilczak, J., Grell, G., Djalalova, I., Peckham, S., Gong, W., Bouchet, V., Moffett, R., Tang, Y., Carmichael, G.R., Mathur, R., Yu, S., 2007. Evaluation of several PM 2.5 forecast models using data collected during the ICARTT/NEAQS 2004 field study. J. Geophys. Res. 112, D10S20. http://dx.doi.org/10.1029/2006JD007608.
Miyakawa, T., Takegawa, N., Kondo, Y., 2007. Removal of sulfur dioxide and formation of sulfate aerosol in Tokyo. J. Geophys. Res. 112 (D13), D13209.
Myles, L.T., Dobosy, R.J., Meyers, T.P., Pendergrass, W.R., 2009. Spatial variability of sulfur dioxide and sulfate over complex terrain in east Tennessee, USA. Atmos. Environ. 43, 3024–3028.
Olivier, J.G.J., Berdowski, J.J.M., 2001. Global emissions sources and sinks. In: Berdowski, J., Guicherit, R., Heij, B.J. (Eds.). The Climate System. A.A. Balkema Publishers/Swets & Zeitlinger Publishers, Lisse, The Netherlands.
Park, R.J., Jacob, D.J., Field, B.D., Yantosca, R.M., Chin, M., 2004. Natural and transboundary pollution influences on sulfate-nitrate-ammonium aerosols in the United States: implications for policy. J. Geophys. Res. 109 (D15), D15204.
Park, R.J., Jacob, D.J., Kumar, N., Yantosca, R.M., 2006. Regional visibility statistics in the United States: natural and transboundary pollution influences, and implications for the regional Haze Rule. Atmos. Environ. 40, 5405–5423.
Rastogi, N., Sarin, M.M., 2005. Long-term characterization of ionic species in aerosols from urban and high-altitude sites in western India: role of mineral dust and anthropogenic sources. Atmos. Environ. 39 (30), 5541–5554.
Rengarajan, R., Sarin, M.M., 2004. Atmospheric deposition fluxes of ^{7}Be, ^{210}Pb and chemical species to the Arabian sea and Bay of Bengal. Indian J. Mar. Sci. 33, 56–64.
Raymond, H.A., Yi, S.-M., Moumen, N., Han, Y., Holsen, T.M., 2004. Quantifying the dry deposition of reactive nitrogen and sulfur containing species in remote areas using a surrogate surface analysis approach. Atmos. Environ. 38, 2687–2697.
Streets, D.G., Zhang, Q., Wang, L., He, K., Hao, J., Wu, Y., Tang, Y., Carmichael, G.R., 2006. Revisiting China's CO emissions after the transport and chemical evolution over the Pacific (TRACE-P) mission: synthesis of inventories, atmospheric modeling, and observations. J. Geophys. Res. 111 (D14), D14306.
Vestreng, V., Klein, H., 2002. Emission Data Reported to UNECE/EMEP. Quality Assurance and Trend Analysis and Presentation of WebDab, MSC-w Status Report 2002. Norwegian Meteorological Institute, Oslo, Norway.
Walker, J.M., Philip, S., Martin, R.V., Seinfeld, J.H., 2012. Simulation of nitrate, sulfate, and ammonium aerosols over the United States. Atmos. Chem. Phys. 12, 11213–11227. http://dx.doi.org/10.5194/acp-12-11213-2012.
Wang, J., Jacob, D.J., Martin, S.T., 2008. Sensitivity of sulfate direct climate forcing to the hysteresis of particle phase transitions. J. Geophys. Res. 113 (D11), D11207.
Wesely, M.L., 1989. Parameterization of surface resistances to gaseous dry deposition in regional scale numerical models. Atmos. Environ. 23, 1293–1304.
Yi, S.M., Holsen, T.M., Noll, K.E., 1997. Comparison of dry deposition predicted from models and measured with a water surface sampler. Environ. Sci. Technol. 31 (1), 272–278.
Zeller, K., Donev, E., Bojinov, H., Nikolov, N., 1997. Air pollution status of the Bulgarian govedartsi ecosystem. Environ. Pollut. 98, 281–289.
Zhang, Y., Carmichael, G.R., 1999. The role of mineral aerosol in tropospheric chemistry in east Asia – a model study. J. Appl. Meteorol. Am. Meteorol. Soc. 353–366.